CONF-8409130-5

NOTICE
PORTIONS OF THIS REPORT ARE ILLEGIBLE.
It has been reproduced from the best
available copy to permit the broadest
possible availability.

FUNDAMENTAL ASPECTS ON ION-BEAM SURFACE MODIFICATION: DEFECT PRODUCTION AND MIGRATION PROCESSES*

L. E. Rehn, R. S. Averback and P. R. Okamoto
Materials Science and Technology Division
Argonne National Laboratory
Argonne, IL 60439

FINAL

CONF-8409130--5

September 1984

DE85 000093

The submitted manuscript has been authored by a contractor of the U. S. Government under contract No. W-31-109-ENG-38. Accordingly, the U. S. Government retains a nonexclusive, royalty-free license to publish or reproduce the published form of this contribution, or allow others to do so, for U. S. Government purposes.

DISCLAIMER

This report was prepared as an account of work sponsored by an agency of the United States Government. Neither the United States Government nor any agency thereof, nor any of their employees, makes any warranty, express or implied, or assumes any legal liability or responsibility for the accuracy, completeness, or usefulness of any information, apparatus, product, or process disclosed, or represents that its use would not infringe privately owned rights. Reference herein to any specific commercial product, process, or service by trade name, trademark, manufacturer, or otherwise does not necessarily constitute or imply its endorsement, recommendation, or favoring by the United States Government or any agency thereof. The views and opinions of authors expressed herein do not necessarily state or reflect those of the United States Government or any agency thereof.

Invited paper submitted to the International Conference on Surface Modification of Metals by Ion Beams, University of Heidelberg, September 17-21, 1984.
*Work supported by the U. S. Department of Energy.

MASTER

DISTRIBUTION OF THIS DOCUMENT IS UNLIMITED

FUNDAMENTAL ASPECTS OF ION-BEAM SURFACE MODIFICATION: DEFECT PRODUCTION AND MIGRATION PROCESSES*

L. E. Rehn, R. S. Averback and P. R. Okamoto
Materials Science and Technology Division
Argonne National Laboratory
Argonne, IL 60439

Abstract

Ion-beam modification of metals is generating increasing scientific interest not only because it has exciting technological potential, but also because it has raised fundamental questions concerning radiation-induced diffusion processes. In addition to the implanted species, several defect production and migration mechanisms contribute to changes in the near-surface composition of an alloy during ion bombardment, e.g., atoms exchange positions via displacements and replacement sequences; preferential sputtering effects arise; radiation-enhanced diffusion and radiation-induced segregation occur. The latter two defect migration mechanisms are of particular significance since they can alter the composition to depths which are much greater than the implanted ion range. By altering various parameters such as irradiation temperature, ion mass, energy, and current density, and initial alloying distributions, a rich variety of near-surface composition profiles can be created.

We have utilized changes in ion mass and energy, and irradiation temperature to distinguish defect production from defect migration effects. Experimental results are presented which provide a guide to the relative efficiencies of different mechanisms under various irradiation conditions.

*Work supported by the U.S. Department of Energy

Introduction

Because energetic ions can deposit energy at high densities over very short periods of time, ion beams can be used to create highly nonequilibrium alloyed surface layers. On the other hand, irradiation conditions can also be chosen such that the irradiation will actually promote equilibrium distributions of alloying components in surface layers. Ion beams can therefore be used to create a rich variety of modified surfaces, and in fact, a number of significant ion-induced changes in materials properties have been established. Perhaps the most significant discovery is that despite the shallow surface layers ($\lesssim$10 μm) which are produced, long-lasting improvements in performance do occur[1-3]. These findings have inspired a broadly based search for applications of surfaces modified by ion beams. They have simultaneously raised several fundamental questions concerning the relative importance of the competing diffusion mechanisms under various irradiation conditions.

Practical applications of ion implantation began in the semiconductor industry, where only small implanted concentrations (10^{11-14} cm^{-2}) are needed to produce the desired changes in electronic properties. Significantly larger doses (10^{15-18} cm^{-2}) are required to alter most properties of interest in metals. The higher doses mean that such secondary effects as defect production and defect migration processes must be understood, and even utilized, if the benefits of ion implantation are to be maximized for metals applications. The introduction of defects and their subsequent migration during ion bombardment lead to changes in both the microstructure (dislocation density, void growth, surface roughness, etc.) and the distribution of alloying elements in the near-surface region. In this paper, we focus on mechanisms which produce compositional changes during ion bombardment.

The importance of defect production and defect migration during ion irradiation can be seen more clearly with the aid of Fig. 1. Here a typical case of ion implantation, 100-keV C ions impinging on a medium atomic number target such as iron or stainless steel, is illustrated schematically. At low doses and temperatures, such an implantation would produce a Gaussian distribution of atoms centered at a depth of ~100 nm, with a full-width at half maximum of several tens of nanometers.

The displacement of lattice atoms due to collisions with the bombarding ions tends to randomize distributions of alloying elements in specimens with pre-existing concentration gradients. For the example shown in Fig. 1, each C ion induces several thousand exchanges of atoms between lattice sites. Since the number of atomic replacements far exceeds the number of implanted ions, this ion-beam mixing offers a greatly enhanced potential relative to the direct implantation effect for altering near-surface compositions.

The production of lattice defects due to collisions of the C ions with target atoms also causes approximately three atoms to be sputtered from the surface of the target for each implanted ion. In most ion bombardment cases the sputter yield, i.e. the ratio of sputtered to implanted atoms, exceeds unity, sometimes by as much as a factor of 100. Preferential sputtering effects can alter the near-surface concentration in alloys; in fact, the relative sputtering yield of target and implanted elements dictates the maximum concentration which can be implanted directly. Since the number of sputtered atoms exceeds the number of implanted ions, the potential for altering the near-surface concentration by sputtering also exceeds the direct implantation effect.

In addition, each C ion produces an average of ~300 vacancy and 300 interstitial defects before coming to rest. At temperatures where the defects are mobile, their migration through the lattice induces mass transport. If the compositional distribution in the target is already in equilibrium, this radiation-enhanced diffusion (RED) will leave the near-surface composition unaltered. In targets with nonequilibrium alloy distributions, RED will accelerate the approach to the equilibrium state.

If the vacancies and/or interstitials preferentially migrate via particular alloying elements, then defect migration will also produce radiation-induced segregation (RIS). Because of the preferential coupling of some alloying components to the defect fluxes, certain elements will be swept into or out of regions which experience a net influx or outflow of defects, producing nonequilibrium segregation effects during irradiation. Once again, since the number of defects which are generated far exceeds the number of implanted ions, both RED and RIS offer enhanced potential for modifying the near-surface composition of metals during ion bombardment.

In the remainder of this paper we discuss some recent results which provide information on the relative importance of ion-beam mixing, sputtering, RED, and RIS under various irradiation conditions.

Defect Migration Processes (RIS and RED)

The impact of RIS on ion-beam surface modification was reviewed in detail a few years ago[4]. We therefore begin with a brief summary of general features, then turn to a discussion of more recent results.

As discussed in the introduction, RIS alters the local composition in regions which experience a net influx or outflow of defects. This redistribution of alloying elements is frequently strong enough to induce precipitation in normally single-phase alloys, and to redistribute phases in multi-phase materials. In general, undersize solutes segregate in the same direction as the defect fluxes and oversize solutes segregate in the opposite direction; it has been argued elsewhere that this strong size-effect correlation implies that interstitial fluxes generally dominate the segregation process during irradiation at elevated temperatures[5]. Another important feature is that RIS occurs regardless of the initial distribution of solute. Although it has been studied most frequently in alloys in which the components were homogeneously distributed before bombardment, significant effects of RIS have been observed in the depth distribution of implanted solutes[6], as well as in the distribution of solute atoms which were introduced by ion-beam mixing of a thin surface layer[7]. RIS of solute that was present initially on the specimen surface because of vacuum contamination has also been reported[8].

The spatial redistribution of alloying components by RIS is determined by the location of both sources and sinks for defects. For shallow depths, the external surface serves as a dominant sink. Hence, RIS generally produces enrichment of undersize solute atoms and a depletion of oversize solute atoms near the surface. During ion irradiation, particularly steep gradients in defect production occur on both sides of the peak damage region, causing undersize solute to be transported out of, and oversize solute to be transported into, the peak damage region[9]. These effects are illustrated in Figs. 2 and 3. Fig. 2 is a dark-field micrograph taken with an Ni_3Si superlattice reflection of a cross-section specimen of Ni-12.7 at %Si after

irradiation with 250 keV protons at 500°C[10]. Visible in the micrograph are, a) a continuous coating of Ni_3Si formed on the surface because of RIS of undersize Si atoms, b) a subsurface layer depleted in Si and, c) a peak damage region highly depleted in Si. Fig. 3 shows concentration profiles of four oversize solutes in nickel measured by Marwick et. al.[6] after bombardment of the specimen with 1.6 x 10^{16} cm^{-2}, 75-keV Ni ions at 500°C. The peak in solute enrichment at ~20nm reflects the outflow of defects from the underlying peak in the point defect concentrations.

Both RIS and RED depend directly on the number of freely migrating defects introduced during irradiation. Hence, both effects exhibit similar functional dependences on irradiation parameters which affect defect migration. Significant defect fluxes are produced during irradiation only when both types of defects, i.e., vacancy- and interstitial-types, are mobile. Otherwise recombination dominates and little long-range mass transport occurs. The temperature range in which RIS and RED can produce redistribution of alloying components over significant distances is therefore the same as for void swelling, approximately 0.3 to 0.6 of the absolute melting temperature.

Recombination of irradiation-induced vacancies with interstitials increases with increasing dose rate. Since recombination reduces the defect concentration, RIS and RED per unit dose decrease with increasing dose rate when recombination dominates defect annihilation, i.e., at lower temperatures. Current theory predicts[11], and experiment confirms[12], that the concentration of freely migrating defects varies inversely as the square root of the dose rate in the recombination-limited temperature regime. Since the steady state vacancy concentration during irradiation at high temperatures is approximately equal to the equilibrium vacancy concentration, the amount of defect annihilation per unit dose is independent of dose rate, and no effect

of dose rate on RIS or RED per unit dose is observed at high temperatures[12].

Recently, we[13] have used in situ measurements of the growth rates of radiation-induced surface coatings (cf. Fig. 2) formed on Ni-12.7 at. % Si alloys to extract the relative efficiencies of different ions for producing freely migrating defects, i.e. defects which are free to induce compositional changes at elevated temperatures via RIS and RED. The results are shown in Fig. 4, where the relative efficiencies (normalized to that of 1 MeV protons) are plotted as a function of the defect-production-weighted, average recoil energy, $P_{1/2}$. The energy and identity of the ions used in each measurement are also indicated on the figure. The abscissa is plotted on a logarithmic scale. $P_{1/2}$ is that primary recoil energy above and below which half of the defects are produced. It gives a measure of the spatial distribution of the defect production; the larger $P_{1/2}$, the greater the tendency for defects to be produced in cascades rather than as isolated defects. Note that $P_{1/2}$ increases with increasing ion mass and energy. A detailed discussion of $P_{1/2}$ can be found in Ref. 14.

Fig. 4 provides a quantitative representation of the relative efficiency for producing RIS and RED as a function of the "hardness" of the primary recoil spectrum. Irradiations with weighted average recoil energies of 1.8, 2.7, 51 and 74 keV are respectively only 48,27,8 and $< 2\%$ as effective as an irradiation with a weighted average recoil energy of 730 eV for introducing defects which are free to migrate long distances. Note that the most rapid decrease in efficiency occurs over recoil energies up to about 5 keV. Muroga et. al.[15] have shown that the efficiency approximately doubles in going from 1 MeV protons to 1 MeV electrons, where all defects are generated by primary recoils $\leq$80eV.

Qualitatively, defect production as a function of primary recoil energy is known to occur as follows. As recoil events increase in energy from tens to hundreds of electrons volts, Frenkel pair production changes from the introduction of randomly distributed, isolated Frenkel defects to the generation of several defect pairs in close proximity. Cascade regions can be clearly distinguished in computer simulation studies for primary recoil energies above about 1 keV, and the size of the cascade then continues to increase with increasing energy. For recoils greater than many keV, the increase in spatial correlation among the defects with increasing recoil energy slows because of the increasing probability for subcascade formation. These qualitative trends are all reflected in the results shown in Fig. 4. More importantly, however, these results provide a quantitative basis for normalizing microstructural changes due to RED or RIS in irradiation environments characterized by widely different primary recoil spectra.

Ion-Beam Mixing

The ability of ion-beam mixing to create highly nonequilibrium alloys over a wide range of carefully controllable compositions using beams of easily generated ions has greatly expanded the potential applications of ion-beam surface modification. Considerable experimental effort over the last few years is now providing information about the fundamental processes by which ions "mix" layers of various materials. We begin with a brief summary of trends which have been observed experimentally, then discuss the relative importance of the different contributing mechanisms under various irradiation conditions. Unless otherwise noted, the statements apply to metal systems, and for temperatures at and below room temperature, where the vast majority of mixing experiments have been performed. An extensive compilation of experimental data on mixing in metals, semiconductors, and oxides has recently been given by Paine and Averback[16].

Typical mixing experiments employ either marker (a thin, ~ 1 nm layer embedded in an otherwise homogeneous host) or layered (two or more layers of different materials each several tens of nanometers thick) specimens prepared by thermal evaporation or sputter deposition. The specimens normally contain very small grains (10-100nm), and unstated impurity levels. Marker layers generally remain Gaussian during spreading, whereas layered specimens yield either error function concentration profiles, or regions of nearly constant composition indicating phase formation.

Mixing of both marker and bilayer specimens is essentially independent of temperature below 100K; the lone exception is the impurity-sensitive step increase in mixing at ~25K in Fe-Pt alloys reported by Bottiger et al.[17] Significant temperature dependent effects have been observed beginning as low as 160K in Ni-Si[18], and as high as 570K in Nb-Si.[19] In metals the mean square diffusion length, $\langle x^2 \rangle$, increases linearly with dose. Mixing per unit dose was independent of ion current (dose rate) in the few examples investigated[17,20].

The amount of mixing varies significantly less between different metal systems than it does in semiconductors. Measured values of $\langle x^2 \rangle / 4\phi F_D$ lie between 0 and 30Å^5/eV below 100K[16]. Here, ϕ is the ion dose per unit area, and F_D is the damage energy deposited per unit path length traversed by the ion. Dividing by ϕ removes the linear dependence of $\langle x^2 \rangle$ on dose which is almost always observed; dividing by F_D normalizes all irradiations to the same energy deposited in nuclear collisions. Hence $\langle x^2 \rangle / \phi F_D$ is a convenient quantity for comparing different mixing experiments.

However, mixing increases faster than linear with F_D. This can be seen in Fig. 5, where results from two different groups[21,22] are shown plotted versus F_D on a log scale. Increasing F_D means that more energy is deposited

in nuclear collisions per unit path length, i.e. that the resulting cascade events are more energetic. Thus the dependence of ion beam mixing on cascade energy density is opposite to that found for RED and RIS (Fig. 4). Energetic cascades produce more mixing per unit of deposited damage energy, but fewer freely migrating defects.

Chemical effects on mixing have been reported even at low temperatures. Averback et al.[23] have shown that the mixing of a Cu isotope in a Cu host is identical for marker and bilayer specimens. However, when bilayers of similar atomic masses are irradiated at 90K, Cheng et al.[24] find that the mixing varies essentially linearly with the heat of mixing calculated using the theory of Miedema. For small heats of mixing, Van Rossum et al.[25] report that mixing varies inversely with the sublimation energies of the materials. Averback and Thompson[23] have shown that room temperature irradiation with 1-MeV Kr ions produced mixing of elements (Cu isotope and Au) which are miscible with Cu, but not of elements (Bi, Mo and Nb) which are immiscible in the solid state. At 6K, all systems mixed except Cu-Mo, which is immiscible in both the liquid and solid states.

Useful clues about ion-beam mixing mechanisms are contained in the experimental results summarized above. One important conclusion is that the main contribution to mixing (at and below room temperature) is clearly an intra-cascade effect. We include within the intra-cascade definition all contributions to mixing from the induced migration of defects formed within the current cascade volume by previous irradiation. The intra-cascade interpretation follows directly from the observed increase in mixing per unit dose with increasing F_D (Fig. 5). As discussed in the previous section, inter-cascade effects like RED and RIS (Fig. 4) decrease with increasing cascade energy density. Further support for the intra-cascade

interpretation of mixing is given by the observed independence of $\langle x^2 \rangle / \phi$ on dose rate, which shows that the effects of one cascade are not influenced by processes occuring in other cascades.

The observed chemical effects therefore imply that thermodynamic driving forces are important within individual cascades even at low (<100K) irradiation temperatures. This conclusion has provided new interest in a classical problem in irradiation effects, i.e. the time development and decay of energetic collisional events in solids. Although current calculations apply only to pure materials and relatively low energy events, computer simulations using molecular dynamics provide perhaps the most detailed guide to what actually occurs within the lifetime of individual cascades.[26,27] The simulations show that the initial kinetic energy of the primary knock on atom is distributed via target atom collisions in a time of $\sim 10^{-13}$s, creating a cascade region containing a very high density of mostly unstable defects. During this "collisional" phase, the average kinetic energy of the atoms within the cascade greatly exceeds their average potential energy. In a subsequent time of $\sim 10^{-12}$s, many of the defects are eliminated by spontaneous recombination events. At the end of this second phase, the point defect concentration is approximately equal to that obtained from the Kinchin and Pease expressions; the average kinetic and potential energies of the cascade atoms are about equal, although both are considerably greater than typical thermal energies. In the final phase (lasting $\sim 10^{-11}$s), some recombination of migrating defects occurs, and the excess energy spreads into the surrounding lattice. Interstitials appear to migrate normally during the cascade cooling phase, but enhanced vacancy migration is observed in the computer simulations.

Recently, Peak and Averback[28] have developed a model of mixing in

collision cascades based on the molecular dynamics picture just described. Mixing in the first two phases of the cascade is considered as ballistic and calculated using linear transport theory, while that in the cooling phase is attributed to a thermal spike. The cascade contains mobile reacting defects, and cools by thermal diffusion. Hence, transport in the spike is similar to RED, but at transiently high temperatures and defect concentrations. Their results suggest that interstitial migration effects during the cascade cooling phase are plausibly at least as important to mixing as ballistic effects. Of course, chemical effects emerge naturally from their model.

Hence, current theories are capable of rationalizing the magnitudes and trends observed in mixing experiments, but a detailed understanding is lacking. For example, Peak and Averback[28] further conclude that "normal" vacancy migration, because of its relatively high activation enthalpy, does not contribute significantly to mixing within cascades. On the other hand, the experimental evidence that the mixing of a Cu-isotope marker in Cu is the same as for a Au marker[23,16] argues strongly against interstitialcy migration as the dominant contribution. Simply stated, the argument goes as follows. Interstitials should produce very rapid dispersal of an isotopic marker via the normal interstitialcy migration mechanism, but should contribute much less to the spreading of oversize marker atoms such as gold in copper since the lattice positions of oversize atoms are believed to be unchanged by passage of an interstitialcy flux[5].

Independent, although quite limited evidence exists which suggests that the enhanced vacancy migration in cascades observed via molecular dynamics may provide the largest contribution to mixing at low temperatures. In situ studies using the ANL HVEM ion interface have demonstrated that in Cu[29] and Cu_3Au[30], vacancy-rich cores within individual ion-induced cascades can

collapse into two-dimensional dislocation loops even at temperatures <30 K. In Fe[31] and Ni[29], however, the collapse of individual cascades is not observed at low temperatures. In the compilation of low temperature mixing data by Paine and Averback[16], it is intriguing to note that the measured mixing in the two systems (Fe and Ni) which do not exhibit collapse at low temperatures is only about one-third as large as that in Cu, which does exhibit collapse.

Sputtering

Strictly speaking, changes in composition due to preferential sputtering occur if and only if the ejection probabilities are different for the different alloying species[32]. Furthermore, the direct effect of preferential sputtering alters the target composition only to the depth from which the sputtered atoms are ejected[33]. Preferential sputtering is very difficult to identify, since at least five additional processes, ion implantation, Gibbsian adsorption, displacement mixing, RED and RIS, contribute to compositional changes in the near-surface region[32,34].

One approach to solving this problem is to note that only the two defect-flux driven effects, RED and RIS, can produce compositional changes at depths significantly greater than the implanted ion range. A primary objective of our work is to obtain relevant parameters for RED and RIS by measuring the kinetics of compositional changes well beneath the ion implanted layer, and to utilize these parameters in the phenomenological model of sputter-induced compositional changes developed by Lam and Wiedersich[34] to assess the contributions from RED and RIS within the implanted layer. A second important motivation for this effort is that the large effects which are observed offer a means for modifying surface layers which are very much thicker than the ion penetration depth[35].

The concentrations and mobilities of defects beneath the implanted layer must be high if significant modifications are to occur over appreciable depths. Indeed, large numbers of defects are created in the near-surface region during sputtering. An estimate of the defect production can be obtained by noting that about half as much energy is required to remove an atom from the surface by sputtering as is necessary to displace an atom from a lattice site in the interior of a crystal. Therefore the number of monolayers of defects generated for each monolayer of sputtered atoms is roughly equal to one-half the number of monolayers penetrated by the ion beam. For example, the range of 5-keV Ar ions in a medium atomic number material such as copper is about 10 monolayers (2-3nm). Thus, approximately five monolayers of interstitial defects (and five monolayers of vacancies) are generated for each monolayer of sputtered atoms. The second requirement, i.e. high defect mobility, is fulfilled at elevated temperatures, where the mobility of both vacancy and interstitial defects in metals can be very high. This is illustrated in Table I, where the calculated root-mean-square diffusion distances, $\langle x^2 \rangle^{1/2}$, for vacancy defects with migration enthalpies, H_m^V, of 0.6 eV (Al) and 1.1 eV (Ni)[36], are tabulated for a diffusion time of one second. We have used:

$$\langle x^2 \rangle = 4Dt \quad \text{and} \quad D = a_o^2 \, \nu_o \exp [- H_m^V / kT];$$

t is the time; a_o is the lattice parameter; ν_o is the preexponential jump frequency (5×10^{13} s^{-1}); T is the absolute temperature.

Table 1. Root-mean-square diffusion distances for a vacancy in one second.

H_m^v	0.6 eV	1.1 eV
$\langle x^2 \rangle^{1/2}$ (500°C)	63 μm	1 μm
$\langle x^2 \rangle^{1/2}$ (600°C)	106 μm	3 μm

The diffusion distances for interstitial atoms, which typically have significantly lower migration enthalpies, are even larger.

Of course actual defect mobilities depend sensitively on the degree of clustering of like defects. Transmission electron microscopy studies of ion bombarded pure copper[37] and pure nickel[38] specimens indicate that even fairly large defect clusters are unstable at temperatures > 400°C. A second important factor is that because the ion bombardment produces a continuous source of defects in the implanted layer, the defect fluxes into the specimen interior are persistent. Consequently, large numbers of both irradiation-induced vacancies and interstitials can escape deep into the interior of metal specimens at temperatures > 400°C.

We have used Auger electron spectroscopy (AES) and ion sputtering at room temperature to depth-profile subsurface changes produced in a Cu-40 at.% Ni specimen by 5-keV Ar bombardment at elevated temperatures. Details of the experimental procedure can be found elsewhere[39]. After 5-keV Ar bombardment at 600°C for two hours at a dose rate of 1.2×10^{15} ions$\cdot$cm$^{-2}\cdot$s^{-1}, nickel enrichment extending several μm's into the specimen was observed. Measurements of the excess nickel concentration found at various depths after two hours of bombardment at 500 and 600°C are shown in Fig. 6. Here, the difference between the nickel concentration measured after the indicated

sputtering time and that measured after sputtering deep into the bulk alloy is plotted on a logarithmic scale as a function of sputtering time at room temperature. The sputtering rate at room temperature is calculated to be ~0.55 nm s^{-1}. Preferential removal of copper during sputtering of Cu-Ni alloys is well known[33]. However, for the conditions found in Fig. 6, i.e. net concentration changes $\leq$ 15% and no abrupt change in composition with depth, the differences in the nickel concentrations measured after sputtering at room temperature are essentially equal to the differences which would be obtained if no preferential sputtering occurred.

The first data point given in Fig. 6 was obtained at a depth of ~6 nm. Hence, all the nickel enrichment depicted in Fig. 6 occurs at depths greater than the ion range ($\leq$ 3nm). The results show two different regions of nickel enrichment extending well beneath the implanted layer. The first region exhibits a relatively steep drop in nickel enrichment (from ~15 at.% to 6 at.%) over depths extending from about 6 to ~50 nm (~90 s of sputtering), while the second region manifests itself as a considerably shallower concentration gradient extending several μm's into the specimen. The primary mechanism responsible for Region I is RED. This situation has been treated by Ho[40], and subsequently by several other authors[41-43]. Assuming that the diffusion in the subsurface is enhanced uniformly, the radiation-enhanced diffusion coefficient, D, can be shown to equal the product of the altered layer thickness, δ, which is defined as the inverse of the slope in Region I, and the surface recession velocity, $\dot{x}$ resulting from sputtering.

We have shown elsewhere[35] that RIS is primarily responsible for Region II. The high production rate of point defects in a thin surface layer combined with the high mobilities of both the vacancy and interstitial defects (see Table I) generate significant defect fluxes which penetrate deep into the

specimen interior. Preferential transport of nickel in the direction of these defect fluxes produces a region of nickel enrichment which extends well beyond the depths to which radiation-enhanced diffusion processes can compete with the rate of surface recession. The existence of these large and persistent defect fluxes at intermediate temperatures provides a means for modifying μm-thick layers during low-energy ion bombardment.

Similar experiments were performed on a Ni-12.7 at.% Si alloy[44]. Region I was clearly observed, but no evidence for a second, deeper region due to RIS was found. This was somewhat surprising, since other RIS effects are known to be strong in Ni-Si alloys. The explanation proposed for the absence of Region II was that the Si reduced the defect mobility, preventing significant defect fluxes into the specimen interior. To test this hypothesis, we have recently performed experiments on a Cu-37 at.% Ni alloy containg 3 at.% Si. Only very weak indications for Region II were observed in the ternary alloy, in support of the reduction in defect mobility hypothesis. Hence, the ability to use RIS to modify μm-thick layers using keV ion energies is restricted to certain alloys, but the extent of this limitation is still unclear.

Conclusion

Phenomenological models based on solutions to several simultaneous rate equations have been formulated for determining the influence of various parameters on mass transport during irradiation. An example taken from Wiedersich[45] which summarizes the temperature dependence of the defect production and migration effects is given in Fig. 7. Here, the steady state diffusion coefficient calculated from the analytical solution to the rate equations of Lam et. al.[46] for a 50 nm thick foil of nickel during

irradiation at 10^{-3} displacements per atom (dpa) per second is shown. Further details can be found in Ref. 45. Diffusion due to defect production exceeds that due to thermally activated defect motion up to temperatures (~300°C) where significant vacancy mobility begins. Above 800°C, the irradiation component becomes insignificant compared to the large equilibrium diffusion coefficient.

Although the general trends shown in Fig. 7 have all been confirmed by experiment, the weakness of the current models is that the large number of required input parameters precludes any predictive capability. Experiments such as those described in the previous sections of this paper are providing some of the needed input. For example, the model results in Fig. 7 are for a given calculated displacement rate (10^{-3} dpa.$\bar{s}^{1}$). In fact, most models of irradiation-induced mass transport normalize different types of irradiation on the basis of calculated dpa rates. However, the results presented in Fig. 4 clearly demonstrate that the efficiency of defect migration processes per calculated dpa decreases strongly as the defects are produced in denser cascades. In Fig. 5, we saw that the efficiency of ion beam mixing per dpa increases for denser cascades. In addition to providing clues about the fundamental mechanisms responsible for mass transport in each case, these quantitative results provide a basis for normalizing different types of irradiation particles in model calculations of mass transport during irradiation.

Acknowledgement

We are grateful for many stimulating discussions with our Argonne colleagues on the effects of ion irradiation on materials. Special thanks go to H. Wiedersich for his continuing support throughout the course of this work, as well as for a critical reading of the manuscript.

References

(1) G. K. Hubler, O. W. Holland, C. R. Clayton and C. W. White, eds., Ion Implantation and Ion Beam Processing of Materials (Elsevier Science Publishing Co., New York, 1984).

(2) J. M. Poate, G. Foti and D. C. Jacobson, eds., Surface Modification and Alloying (Plenum Press, New York and London, 1983).

(3) Proceedings of the Conference on Ion Beam Modification of Materials 84 held at Cornell University, July 16-20, 1984, to be published.

(4) L. E. Rehn in: Metastable Materials Formation by Ion Implantation, S. T. Picroux and W. J. Choyke, eds. (Elsevier Science Publishing Company, New York, 1982) 17.

(5) L. E. Rehn and P. R. Okamoto in: Phase Transformations during irradiation F. V. Nolfi, Jr., ed. (Applied Science Publishers, London and New York, 1983) 247.

(6) A. D. Marwick, R. C. Piller and P. M. Sivell, J. Nucl. Mater. 83 (1979) 35.

(7) A. D. Marwick and R. C. Piller: Ion Beam Modification of Materials, R. E. Benenson et al. eds. (North-Holland, New York 1981) 121.

(8) A. D. Marwick in: Ion Beam Modification of Materials, R. E. Benenson et al. eds. (North-Holland, New York 1981) 827.

(9) N. Q. Lam, K. Janghorban and A. J. Ardell, J. Nucl. Mater. 101 (1981) 314.

(10) C. Allen, P. R. Okamoto and N. J. Zaluzec, Argonne National Laboratory, unpublished work.

(11) P. R. Okamoto, L. E. Rehn and R. S. Averback, J. Nucl. Mater. 108 & 109 (1982) 319.

(12) R. S. Averback, L. E. Rehn, W. Wagner, H. Wiedersich and P. R. Okamoto Phys. Rev. B28 (1983) 3100.

(13) L. E. Rehn, P. R. Okamoto and R. S Averback, Phys. Rev. B (1984) in press.

(14) R. S. Averback, R. Benedek, and K. L. Merkle, Phys. Rev. B18. (1978) 4156.

(15) T. Muroga, P. R. Okamoto, and H. Wiedersich, Radiat. Eff. Lett. 68 (1983) 163.

(16) B. M. Paine and R. S. Averback, in Ref. 3.

(17) J. Bottiger, S. K. Nielsen, H. J. Whitlow and P. Wriedt, Nucl. Inst. and Meth. 218 (1983) 684.

(18) L. S. Wielunski, B. M. Paine, B. X. Liu, C.-D. Lien, and M.-A. Nicolet, Phys. Stat. Sol. (a) 72 (1982) 399.

(19) S. Matteson, J. Roth, and M.-A. Nicolet, Rad. Effects 42 (1979) 217.

(20) R. S. Averback, L. J. Thompson, Jr., J. Moyle and M. Schalit, J. Appl. Phys. 53 (1982) 1342.

(21) J. Bottiger, S. K. Nielsen, and P. T. Thorsen, in Ref. 3.

(22) R. S. Averback, L. J. Thompson, Jr., and L. E. Rehn in Ref. 1, p. 25.

(23) R. S. Averback and L. J. Thompson, Jr., unpublished (1984).

(24) Y.-T. Cheng, M. Van Rossum, W. L. Johnson, and M.-A. Nicolet, Appl. Phys. Lett. (1984) in press.

(25) M. Van Rossum, Y.-T. Chen, W. L. Johnson and M.-A. Nicolet, unpublished (1984).

(26) M. W. Guinan and J. H. Kinney, J. Nucl. Mater. 103&104 (1981) 1319.

(27) W. E. King and R. Benedek, J. Nucl. Mater. 117 (1983) 26.

(28) D. Peak and R. S. Averback in Ref. 3.

(29) M. A. Kirk, M. L. Jenkins and I. M. Robertson, (1984) unpublished results.

(30) T. J. Black, M. L. Jenkins and M. A. Kirk Proc. of EMAG 83 (Electron Microscopy and Analysts Group - 1983) Guilford, England 1983.

(31) I. M. Robertson, M. A. Kirk and W. E. King, Scripta Metall. 18 (1984) 317.

(32) H. H. Andersen, J. Vac. Sci. Technol. 16 (1979) 770.

(33) G. Betz and G. K. Wehner in Sputtering by Particle Bombardment II, R. Behrisch, ed., (Springer Verlag, New York, 1983) 11.

(34) N. Q. Lam and H. Wiedersich, J. Nucl. Mater. 103 & 104 (1982) 433.

(35) L. E. Rehn, N. Q. Lam, and H. Weidersich in Ref. 1, p. 37.

(36) R. W. Siegel in Positron Annihilation, P. G. Colemen et al., eds., North Holland Publishing Co., New York, 351 (1982).

(37) C. A. English, B. L. Eyre and J. Summers, Phil. Mag. 34, 603 (1976).

(38) I. M. Robinson and M. L. Jenkins, Phil. Mag. A43, 999 (1981).

(39) L. E. Rehn, S. Danyluk and H. Wiedersich, Phys. Rev. Lett. 43 (1979) 1764.

(40 P. S. Ho, Surf. Sci. 72, 253 (1978).

(41) D. G. Swartzfager, S. B. Ziemecki and M. J. Kelley, J. Vac. Sci. Technol. 19(2), 185 (1981).

(42) R. Webb, G. Carter and R. Collins, Rad. Effects 39, 129 (1978).

(43) H. Wiedersich in Surface Modification and Alloying, J. M. Poate and G. Foti, eds. Plenum Press, New York 1983 261.

(44) L. E. Rehn, V. T. Boccio and H. Wiedersich, Surf. Sci. 128 (1983) 37.

(45) H. Wiedersich in Ref. 3.

(46) N. Q. Lam, S. J. Rothman and R. Sizmann, Radiat. Effects 23 (1974) 53.

Figure Captions

Fig. 1 Schematic illustration of defect production and migration effects on composition during 100-keV carbon ion bombardment of a medium atomic number target. Approximately three atoms are sputtered from the surface, several thousand exchanges of atoms between lattice sites occur, and about 300 vacancy and 300 interstitial defects are produced for each implanted ion.

Fig. 2 Dark-field micrograph of a cross-section specimen of Ni-12.7 at.% Si after bombardment with 250 keV protons at 500°C. RIS of silicon has produced a surface coating of the Ni_3Si phase, and a peak damage region which is highly depleted of Si.

Fig. 3 Depth profiles of four solutes normalized to the bulk concentrations in a nickel alloy after bombardment with 75 keV Ni^{58} ions to a dose of 1.6×10^{16} ions/cm^2. The peak at ~20 nm reflects the subsurface peak in defect concentration.

Fig. 4 Relative efficiencies of various ions for producing long-range migrating defects at elevated temperature plotted as a function of the weighted average recoil energy.

Fig. 5. Measurements of the low-temperature mixing efficiency of several ions plotted as a function of F_D, the energy deposited per unit depth in nuclear collisions. As F_D increases, cascade events become more energetic, and the amount of mixing per unit of deposited damage energy increases.

Fig. 6 Experimental measurements of subsurface nickel enrichment produced by two hours of sputtering with 5-keV Ar ions at 500 and at 600°C.

Fig. 7 The steady state diffusion coefficient in a 50 nm thick foil of Ni at a damage rate of 10^{-3} dpa/s, calculated from the analytical solution to the rate equations due to Lam et al. A sink density of $10^{10}/cm^2$ was asumed. The thermal diffusion coefficient and the diffusion coefficient due to defect production are also shown.

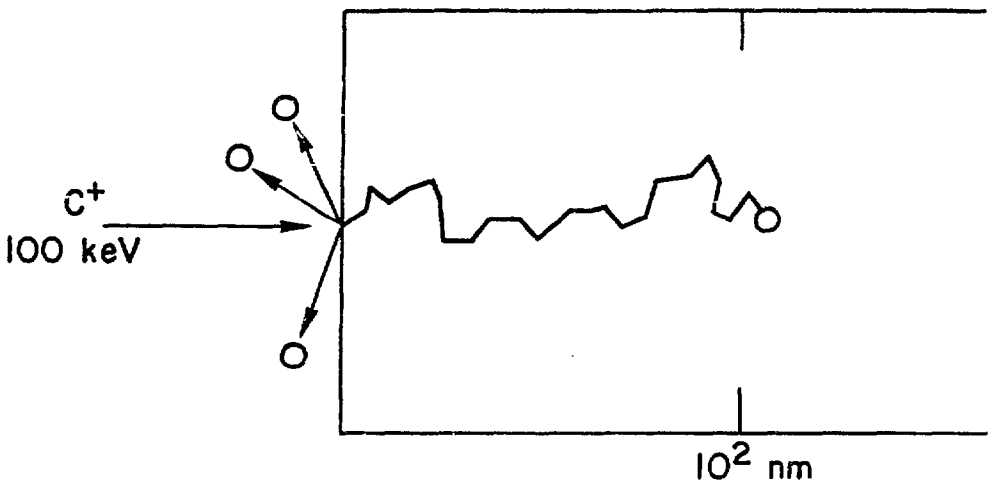

COMPOSITION MODIFIED BY :	PER ION
IMPLANTED ION	1 ATOM
SPUTTERING	~3 ATOMS
ION-BEAM MIXING	MANY ATOMS
RED	~300 DEFECTS
RIS	~300 DEFECTS

Figure 1

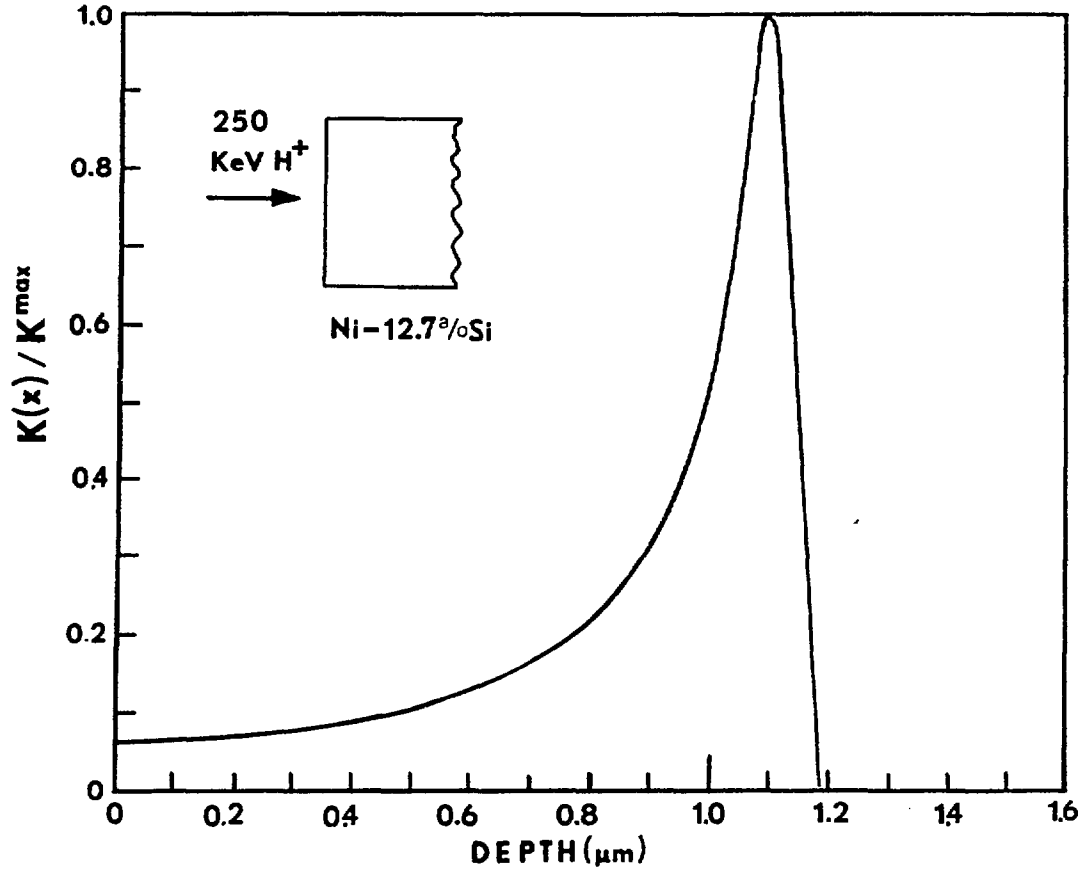
1.0
0.8
0.6
0.4
0.2
0
K(x) / K^max
250
KeV H+
Ni-12.7a/oSi
0
0.2
0.4
0.6
0.8
1.0
1.2
1.4
1.6
DEPTH (μm)

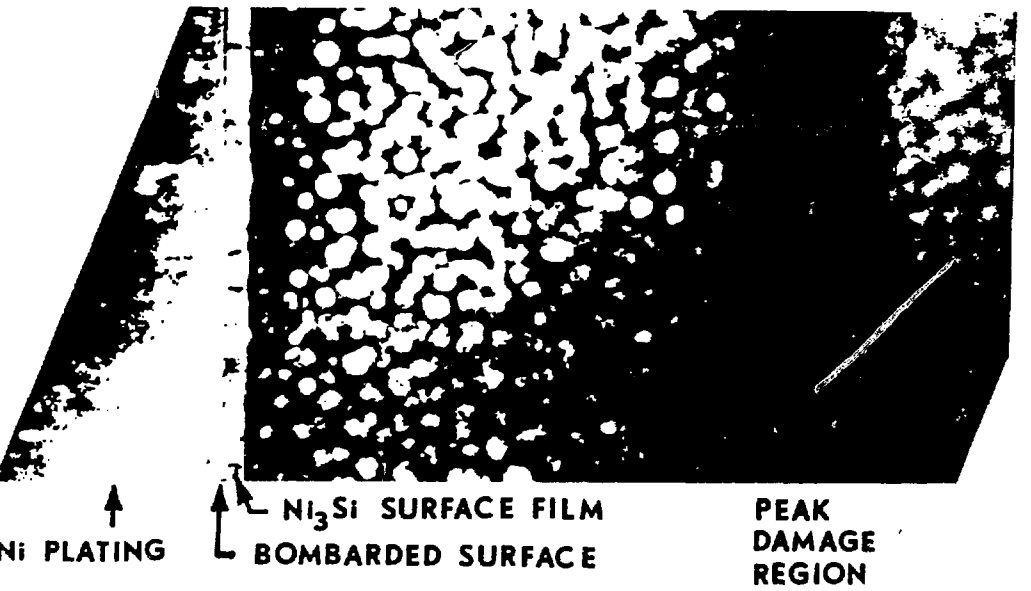
Ni PLATING
Ni3Si SURFACE FILM
BOMBARDED SURFACE
PEAK
DAMAGE
REGION

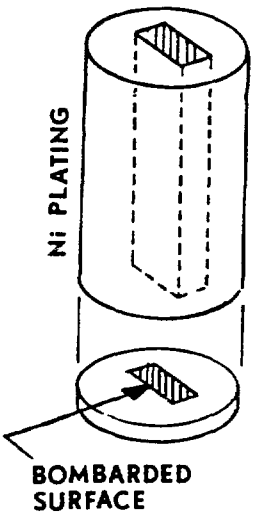
Ni PLATING
BOMBARDED
SURFACE

Figure 2

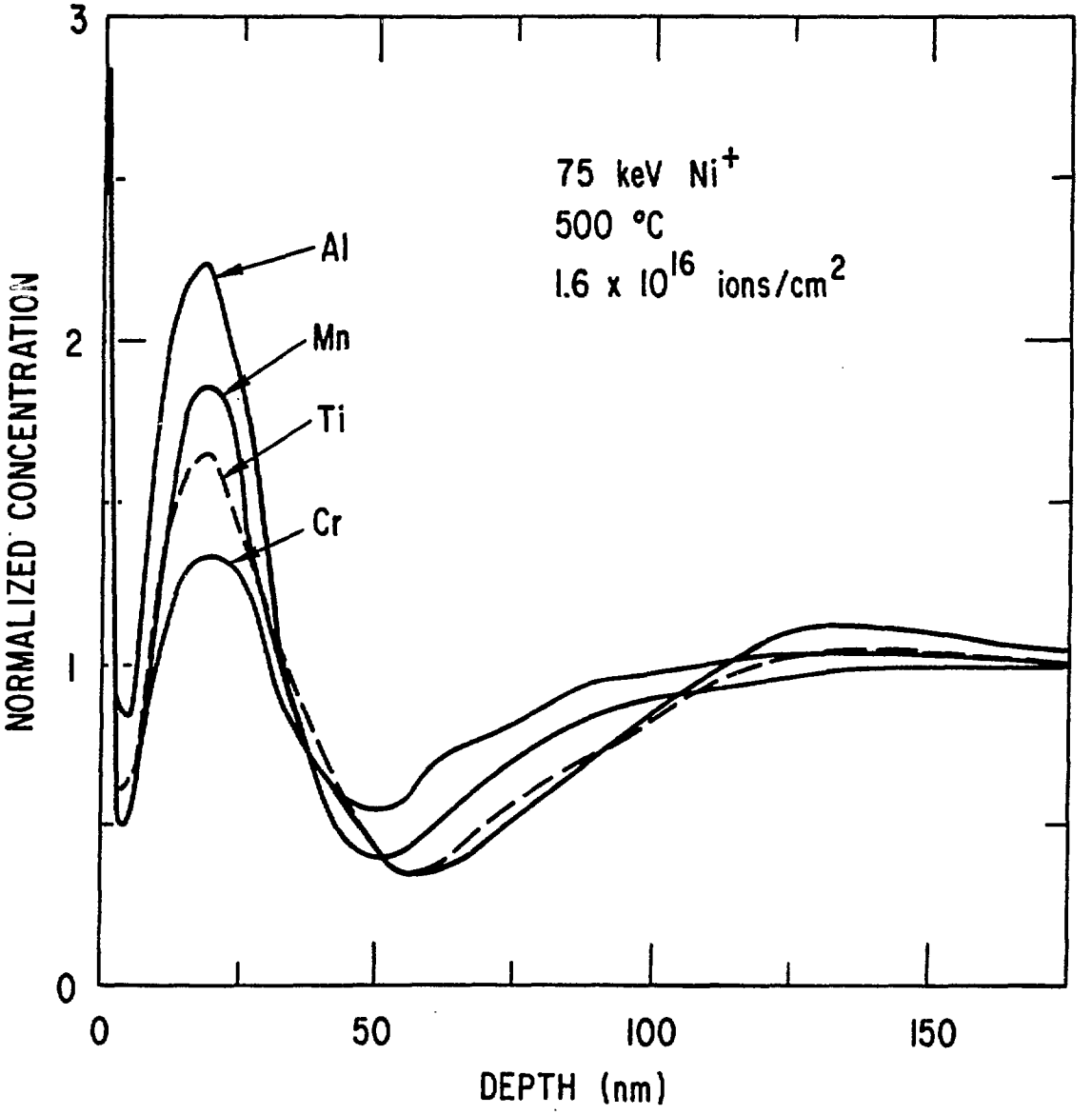
75 keV Ni+
500 °C
1.6 x 10^16 ions/cm^2
Al
Mn
Ti
Cr
NORMALIZED CONCENTRATION
DEPTH (nm)
0
1
2
3
0
50
100
150

Figure 3

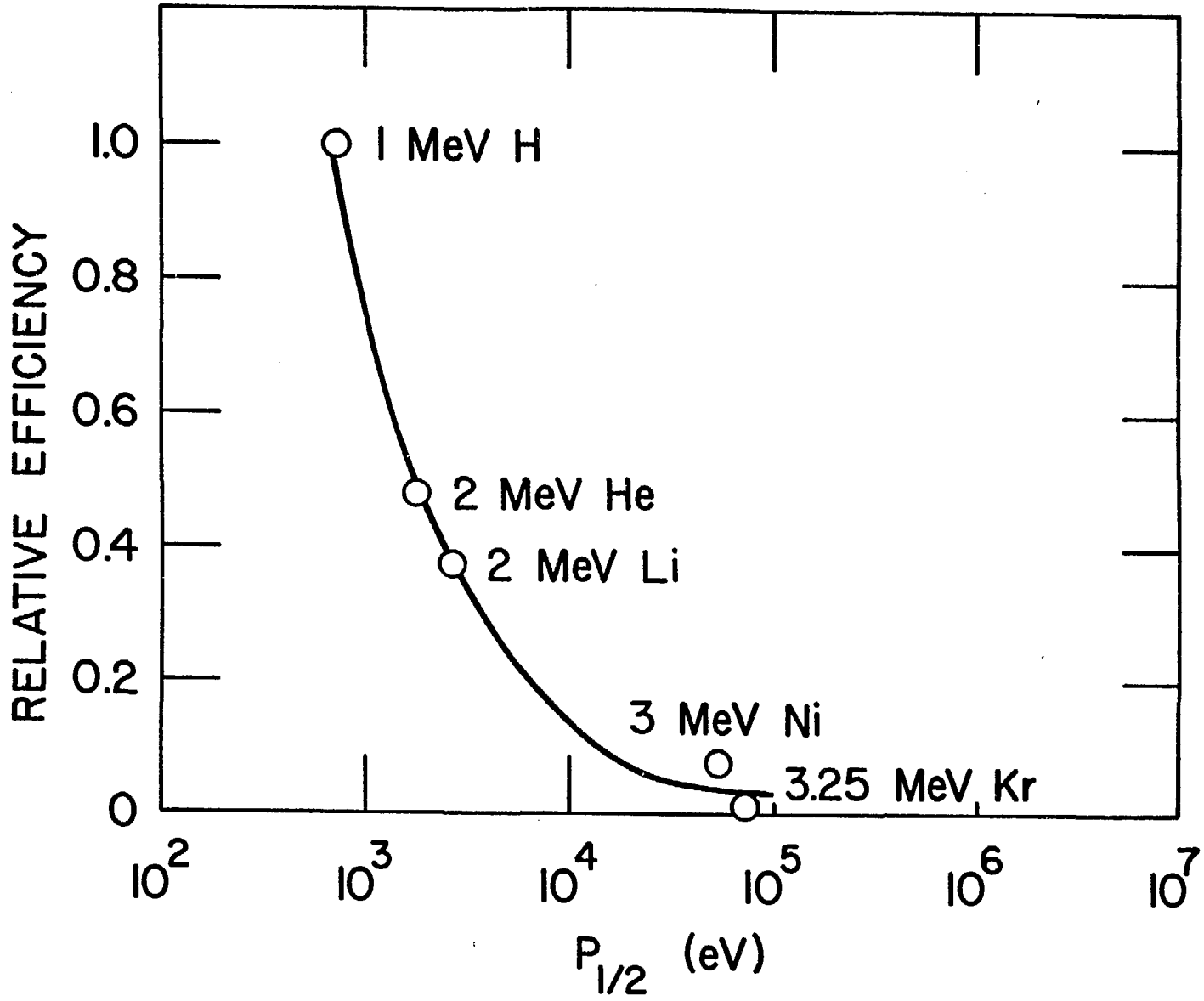
RELATIVE EFFICIENCY
1.0
0.8
0.6
0.4
0.2
0
1 MeV H
2 MeV He
2 MeV Li
3 MeV Ni
3.25 MeV Kr
10^2
10^3
10^4
10^5
10^6
10^7
$P_{1/2}$ (eV)

Figure 4

(4)

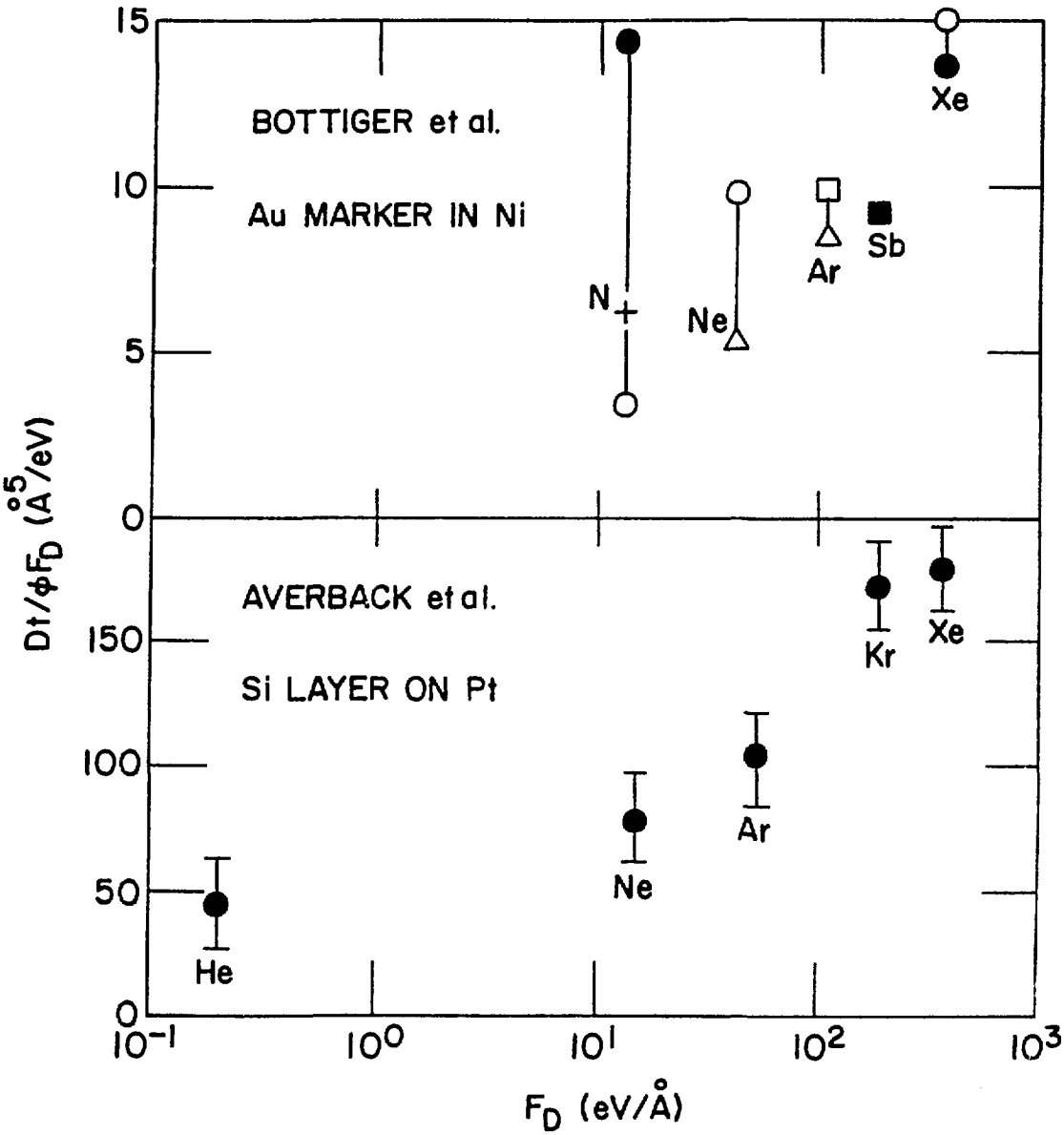
BOTTIGER et al.
Au MARKER IN Ni
AVERBACK et al.
Si LAYER ON Pt
Xe
Sb
Ar
N
Ne
Kr
Xe
Ar
Ne
He
15
10
5
0
150
100
50
0
10^{-1}
10^{0}
10^{1}
10^{2}
10^{3}
$Dt/\phi F_D$ (Å^5/eV)
F_D (eV/Å)

Figure 5

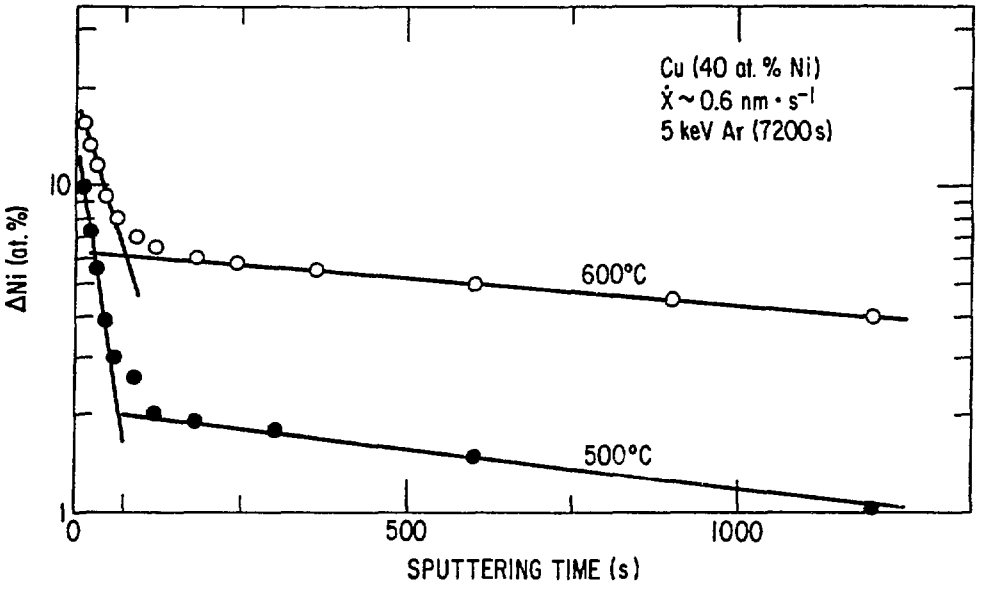
Cu (40 at. % Ni)
$\dot{X} \sim 0.6$ nm · s^{-1}
5 keV Ar (7200 s)
600°C
500°C
ΔNi (at. %)
10
1
0
500
1000
SPUTTERING TIME (s)

Figure 6

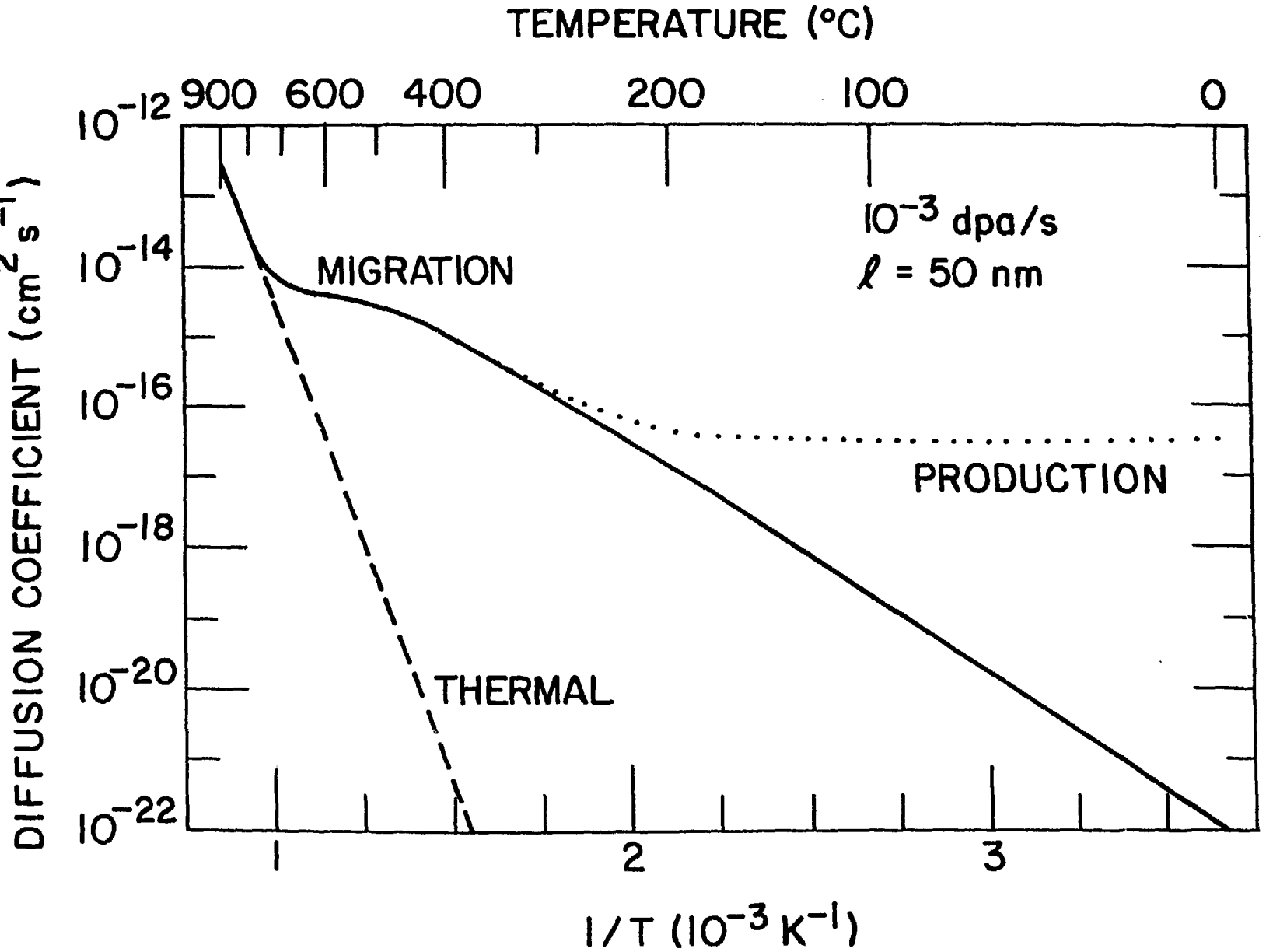
TEMPERATURE (°C)
900
600
400
200
100
0
10^{-12}
10^{-14}
10^{-16}
10^{-18}
10^{-20}
10^{-22}
DIFFUSION COEFFICIENT ($cm^2 s^{-1}$)
10^{-3} dpa/s
ℓ = 50 nm
MIGRATION
PRODUCTION
THERMAL
1
2
3
1/T ($10^{-3} K^{-1}$)

Figure 7